Development and use of an Atomization Model for Transient Evaporative Diesel Sprays

C. Méndez[1], B. Giménez[2] and F. Castro[3]

[1],[2] y [3] IEF – Dpto. Ingeniería Energética y Fluidomecánica. Escuela Técnica Superior de Ingenieros Industriales. Universidad de Valladolid. Paseo del Cauce s/n, E-47011 Valladolid, Spain. Telephone: +(34) 983 423 363. Fax: +(34) 983 423 363.
[1] E-mail: mendez@eis.uva.es
[2] E-mail: blanca@dali.eis.uva.es
SAE member number: 6100191172
[3] E-mail: castro@eis.uva.es

An injection and atomization model for transient evaporative diesel sprays is presented in this work. The model has been developed by accounting for primary and secondary atomization, and droplet-air interaction. Several sub-models are included: A primary atomization model of the liquid vein, based on the jet interface instabilities caused by aerodynamic interaction; A secondary atomization model of droplet break-up, based on Taylor's analogy; A deceleration model based on the aerodynamic drag forces. Spray evolution is based on calculating the lives of characteristic drops parcels, thus giving the model a Discrete Droplet Model type.
To validate the numerical results, some experimental measures have been carried out. Droplet velocity and diameter of a non-stationary evaporative Diesel spray have been measured using a two-component Phase Doppler Anemometer (PDA), as well as the tip penetration by using digital spray images taken with a CCD camera. As a result, the model has shown that the tip penetration can be non linear at the very beginning of the injection. The numerical model is an important tool to study the influence of different operating conditions, such as ambient conditions, liquid properties, injection conditions, etc., without the need of making experimental tests.

1. Introduction

Sprays are especially important in Diesel engines, gasoline engines, gas turbines and rocket engines. It is necessary to obtain a detailed understanding of spray formation and development in order to predict sprays behavior.
During many years, the basic mechanisms of liquid atomization have been under extensive theoretical and experimental investigation ([1], [2], [3], etc.). Knowledge of mechanisms of atomization is important because it is needed to optimize the performance of injection systems. Depending on the mechanism considered as the main one, different atomization models are proposed. Nowadays, most of the models proposed can be included in one of these two general groups: models based on the growing of surface wave instabilities like the Reitz's one [4] and models based on Taylor's analogy [5]. Every model includes adjustable constants to be determined by comparison to experimental data.
The surface wave model proposed by Reitz [4] is based on the growing of Kevin-Helmholtz instabilities upon the liquid surface by means of the aerodynamic interaction with surrounding gas. Starting from a linear stability analysis of a liquid vein [1] a dispersion

equation is derived, which relates the growth of an initial perturbation of infinitesimal amplitude on a liquid surface to its wavelength and other parameters of both liquid and ambient gas. The size of the produced drops is proportional to the wavelength of the fastest growing wave.
Models based on Taylor's analogy break-up (TAB) [5] consider the distortion, deformation and oscillation of a drop analogue to the movement of a mass-shock absorber-hook system. The external force acting the system is analogue to the aerodynamic force, the hook force is analogue to the surface tension forces and the dumping force is similar to the viscous forces.
The present model uses a wave growing model for the atomization of the injected blobs (primary atomization) and a TAB model for the break-up of drops (secondary atomization).

2. Numerical Model Developed

The numerical model developed is a Discrete Droplet Model, that follows the drop trajectory in three dimensions, treating separately the continuous phase from the disperse one. The model injects some cylindrical blobs, at the nozzle location, which will experience a primary atomization process and some drops parcels or smaller blobs are removed from them. Subsequently, the new drops or blobs can experience another primary atomization process, being removed from them drops of smaller size, or may experience a secondary atomization process, being totally broken in smaller drops. In each time step some cylindrical blobs, using an experimental injection velocity law.
Also, all existing drops and blobs (the new ones and the ones injected in previous time steps) are analyzed to determine the atomization process they will be submitted. The criterion used is based on experimental results. If the diameter is larger than a critical one, the blob is submitted to primary atomization, otherwise to secondary atomization. As critical diameter 35 μm was used as it is explained in 3.2.

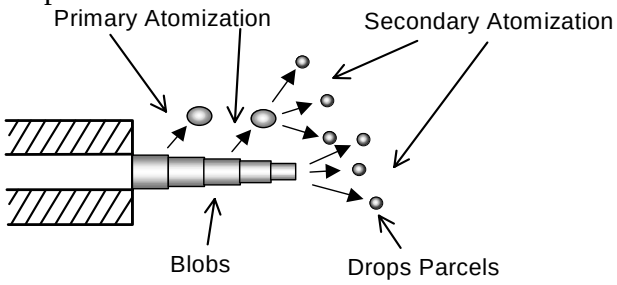

Fig. 1. Scheme of primary and secondary atomization.

Each blob or droplets parcel is submitted to a deceleration process, due to the relative velocity drop-air. The air velocity at each position is computed by a very simple model using momentum transfer from drops to air.

2.1 Primary Atomization

As it has been said, the primary atomization model is based on the model of instabilities growing by Reitz [4]. The maximum growth rate, **Ω**, of the fastest growing wave and its corresponding wavelength, Λ, derived from the dispersion equation, are related to properties of the liquid and the gas [4]:

$$\Lambda = 9{,}02\frac{(1+0{,}45Z^{0,5})(1+0{,}4T^{0,7})}{(1+0{,}8We_g^{1,67})^{0,6}}\cdot a \qquad \Omega = \left(\frac{\rho_l a^3}{\sigma}\right)^{-0,5}\cdot\frac{0{,}34+0{,}38We_g^{1,5}}{(1+Z)(1+1{,}4T^{0,6})} \tag{1}$$

where, a is the blob radius, $Z = \frac{We_l^{0,5}}{Re_l}$; $T = ZWe_g^{0,5}$; $We_l = \frac{\rho_l v_r^2 a}{\sigma}$; $We_g = \frac{\rho_g v_r^2 a}{\sigma}$; $Re_l = \frac{\rho_l v_r a}{\mu_l}$.

Liquid breakup is modeled by postulating that new drops of radius 'r', proportional to the wavelength of the fastest growing wave, are created from the blob being $r = B_0 \cdot \Lambda$ ($B_0 \cdot \Lambda \leq a$).

The value of the constant B_0 is determined by comparison to experimental data. The breakup time is defined by:

$$\tau = \frac{3{,}726 B_1 a}{\Lambda \Omega} \tag{2}$$

where B_1 is a time constant. There are some differences about the value of B_1 depending on the authors and the simulation conditions going from $B_1 = 1$ to $B_1 = 60$ approximately ([5], [6], [7], [8], [9], [10]).

The volume detached from the blob is assumed to be one thorus with circular section, every wavelength (Fig. 2).

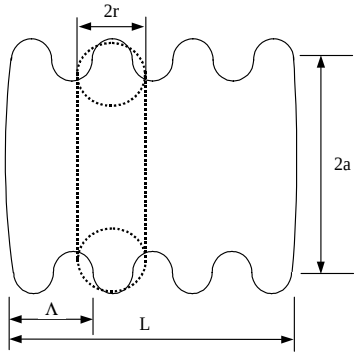

Fig. 2. Scheme of the volume detached

To avoid an excessive discretization, the volume detached is divided into several drops parcels containing drops with characteristic radius $r = B_0 \cdot \Lambda$. The case when $B_0 \Lambda > a$ or the volume detached from the blob larger than the original blob volume, is solve submitting the blob to a secondary atomization process to avoid a non realistic growing of the drops.

2.2. Secondary Atomization

The TAB model is used to represent secondary breakup of droplets into smaller ones. The oscillation of the drop surface is described by a second-order ordinary differential equation:

$$\ddot{y} = \frac{C_F}{C_b} \frac{\rho_g}{\rho_l} \frac{v_r^2}{r^2} - \frac{C_k \sigma}{\rho_l r^3} y - \frac{C_d \mu_l}{\rho_l r^2} \dot{y} \tag{3}$$

being $y = x/C_b a$, x the displacement of the equator of the drop from its equilibrium position, a the radius of the parent drop and C_b, C_F, C_K, C_d constants to be determined by comparison to experimental data. The breakup criterion considers that the drop breaks when $y>1$.

The size of the new created drops is determined by means of an energy balance between the parent total energy before the breaking and the children total energy after breakup [5]. The value of the Sauter mean radius of the created drops is shown in eq (4).

$$r_{32} = \frac{r}{1 + \frac{K}{5} C_b^2 C_k + \left(\frac{K C_b^2}{5} - \frac{C_b^2 C_v^2}{6} \right) \frac{\rho_l r^3}{\sigma} \dot{y}^2} \tag{4}$$

where C_v and K are constants to be determined.

2.3. Drop Drag Model

The equation of motion of a spherical drop moving at relative velocity, V_{rel}, in a gas is:

$$\rho_l V \frac{d^2\overline{X}}{dt^2} = \frac{C_D A_f \rho_g \overline{V}_{rel}^2}{2} \cdot \frac{\overline{X}}{|X|} \tag{5}$$

where $\overline{X}$, V, and A_f are the drop's position, volume, and frontal area, respectively. Instead of consider the drop as a rigid sphere, the present model considers that when a liquid drop enters a gas stream with a sufficiently large Weber number, it deforms and is no longer spherical as it interacts with the gas. To take this deformation in account, an expression proposed by Lee and Reitz [11] is used for the drag coefficient (eq. 6). Using this expression, the coefficient lies between the lower limit of a sphere and the upper limit of a disk. The drag coefficient for the rigid sphere, $C_{D,\,sphere}$, is used the one given by Putnam [12]:

$$C_D = C_{D,sphere}(1 + 2.632y) \qquad C_{D,sphere} = \begin{cases} \dfrac{24}{Re}\left(1 + \dfrac{1}{6}Re^{2/3}\right) & Re \le 1000 \\ 0{,}424 & Re > 1000 \end{cases} \tag{6}$$

The motion equation of a drop (eq. 5) and the deformation equation (eq. 3) are solved in a coupled way.

3. Experiments

Several experiments to validate the numerical results were carried out.

3.1. Experimental Set-up

The experimental set-up consists of an intermittent Diesel injection system. Such a set-up allows for the study of a spray injected at high velocity in an air cross-flow at ambient pressure and temperature (Fig. 3.).

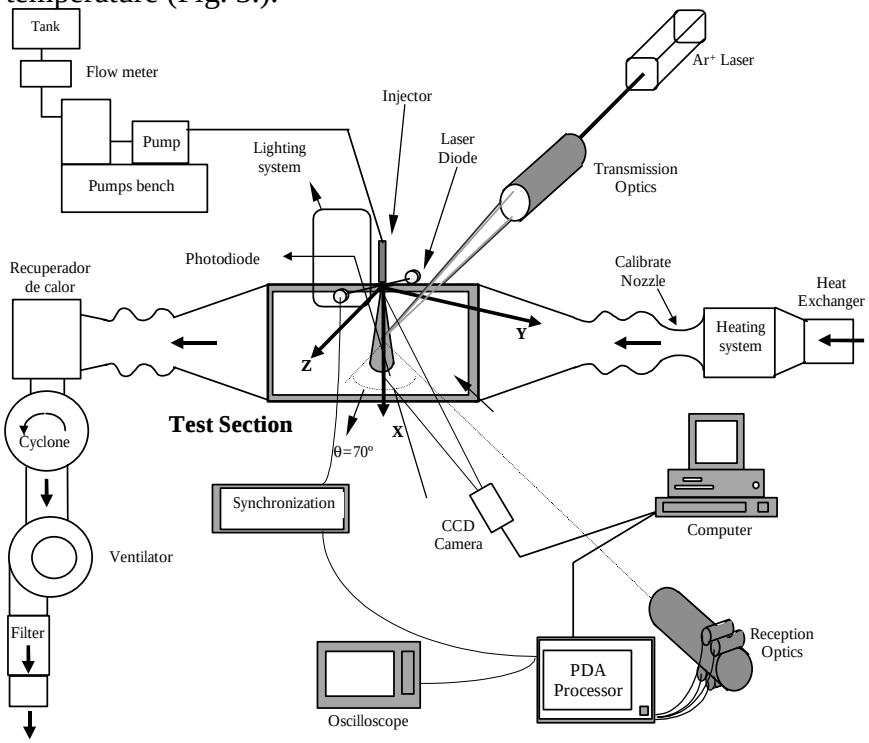

Fig. 3. Scheme of the experimental set-up

The main set-up elements are: a low velocity wind tunnel, an injection system, an injection detection system, an images acquisition system and a two components Phase Doppler Anemometry system (PDA) to make all the measures.
It is possible to obtain two components of the drop velocity (axial and radial) and its diameter.
The low velocity wind tunnel is used to create an air cross-flow, dragging the small drops remaining between two consecutive injections and allowing for the right visualization and measuring of the spray. The velocity is very low not to influence the development of the spray [13].
The injector is placed on the upper part of the test section, such that the spray develops vertically down. The test section includes a 3D displacement system to measure over the whole spray without moving the PDA system.
The injector has a single hole with d_0 = 0,23 mm exit diameter and l_0/d_0 = 4 (being l_0 the exit length of the injector). The acting pressure is 40 MPa (Fig. 4a.)

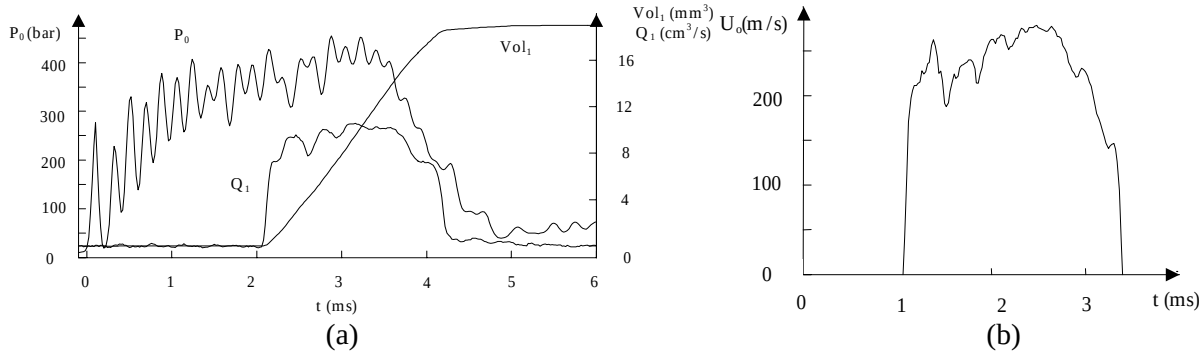

Fig. 4. (a) Pressure P_0, Flow rate Q_1 and Injected volume Vol_1; **(b)** Instant injection velocity

The instant velocity is shown in Fig. 4b and it is the one used to get the numerical results.
Another necessary system of the set-up is the synchronization one to synchronize the data acquisition system to the injection starting time. It was used a detection system consisting of a laser diode and a photodiode.
The set-up also allows for the images acquisition by means of a CCD camera. This system is used to set the spray axis perfectly vertical, to determine the delayed time and to determine the tip penetration of the spray. It is very important to know as close as possible the delayed time to know the exact time of the measures. The delayed time is the time that takes the spray to go from the nozzle exit hole to the laser diode that starts the acquisition.

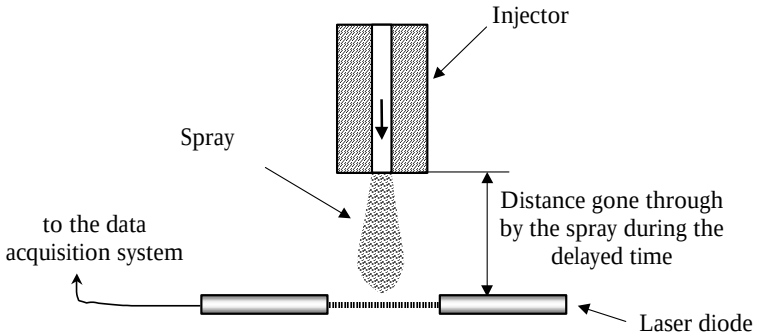

Fig. 5. Scheme of the distance travel through by the spray during the delayed time

Several images of the spray are acquired with the CCD camera in several instants after the spray crosses the laser diode. Making a linear backward extrapolation of the data, the delayed time is determined when penetration is zero. In this case, the estimated value was 110 μs, as it is seen in Fig. 6.

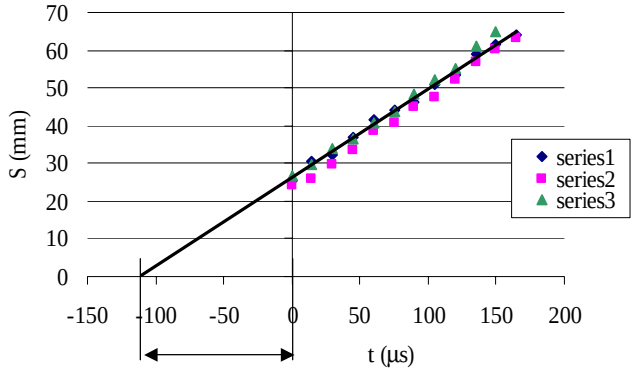

Fig. 6. Determination of the delayed time

3.2. Experiments carried out

The liquid used in the experiments was light Diesel, with the following properties: $\rho_1 = 840$ kg/m^3, $p_v = 80$ kPa, $\sigma = 0{,}016$ N/m and $\mu_1 = 0{,}172 \cdot 10^{-3}$ Pa·s
The common conditions for all experiments are: Temperature: 293 K; Injection Pressure: $P_l = 40$ Mpa; Injection duration: $t_{iny} \approx 2$ ms; Air cross-flow at ambient pressure; Duration of data acquisition temporal window: 50 μs.
The use of such a small temporal window for data acquisition allows for a spray characterization that can be consider instantaneous [13]. But it has disadvantages like the big number of drops rejected for not passing the PDA level validation criteria.
In some previous studies of this Diesel spray [14], the measures of drops with diameter larger than 35 μm were found not to be considered, because its frequency is lower than 1% and they were proved to be optical errors. The effect of these big drops is rather noticeable in the value of the drop mean diameter D_{10}.
The experimental measures carried out were made at several axial locations at 200 μs, 360 μs and 460 μs after injection start. The radial distance between two consecutive measure points was 0,25 mm.

4. Results and discussion

For the validation of the numerical results and determination the constants of models, comparison to experimental data are made. The numerical results of the penetration are shown in Fig. 7a. It is possible to see that penetration is not linear at the beginning of the injection. The importance of the latter is quite high, because the delayed time is longer. Making a displacement in the penetration simulated curve to adapt it to the experimental data, the new estimated delayed time is 195 μs.
Using this new estimated time, the experimental measures at t = 200 μs corresponds to t = 285 μs and measures at t = 360 μs corresponds to t = 445 μs. Penetration has been proved to be highly influenced by the injection law.

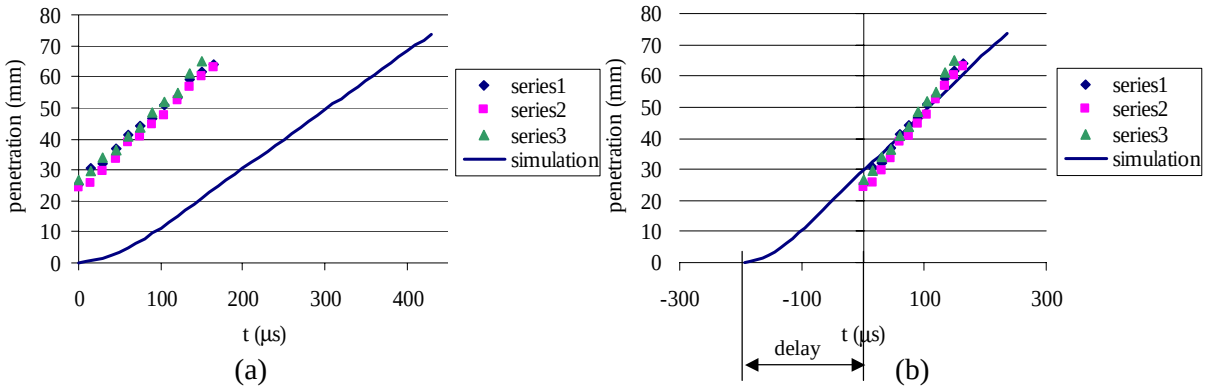

Fig. 7. Determination of the delayed time

It is very difficult to fix the values of the constant of the models, because there exists a big influence of any of them over the others, so results are influenced by combinations of them. After an influencing study and several comparisons to experimental data, the values were adjusted as it is summarized in table 2.

Table 2. Values of the constants

B_0	B_1	C_d	C_k	C_b	C_F	C_v	K
0.6	1.2	5	8	0.6	0.15	1	1.1

In Fig. 8 it is show an example of the image of the spray obtained by numerical simulation at t = 285 μs.

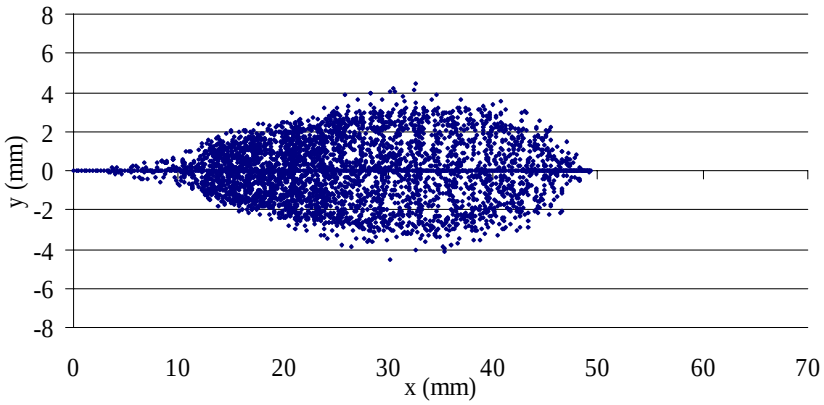

Fig. 8. Numerical image of the spray at 285 μs

Comparing, for instance, the axial velocity at two different axial positions and at two different times after injection it is obtained the Fig. 9.

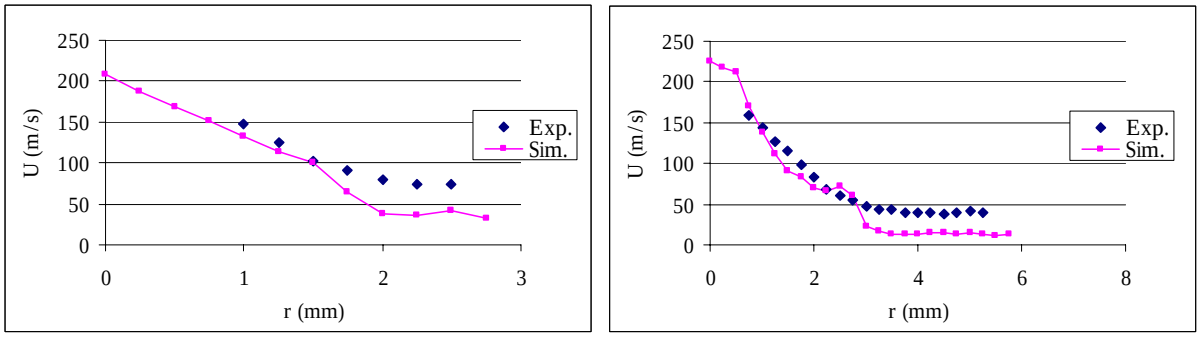

(a) x/d_0 = 160 and t = 285 μs (a) x/d_0 = 240 and t = 445 μs

Fig. 9. Comparison of axial velocity

In both pictures it is seen that while there no exists experimental results at the axis (r = 0 mm) because of the high liquid density, it is possible to get numerical results at that location. The

trend of the experimental axial velocity is followed by numerical results. The axial velocity is decreasing while the radial position is increasing. There are more differences at the higher radial locations, because of the treatment of the air movement. The momentum transfer model for the air velocity is too simple to reproduce the complex air movement inside and around the spray.

In Fig. 10. It is shown another comparison between the arithmetic mean diameter, D_{10}.

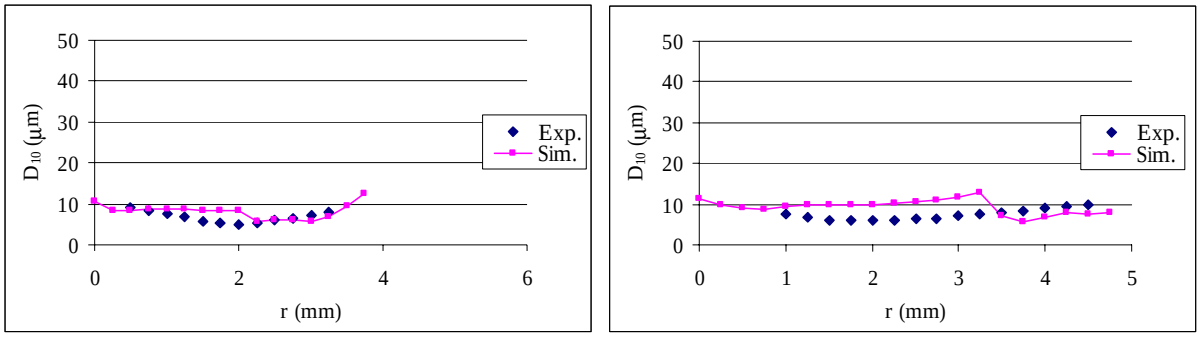

(a) $x/d_0 = 120$ and $t = 285$ µs (a) $x/d_0 = 160$ and $t = 445$ µs

Fig. 9. Comparison of arithmetic mean diameter, D_{10}

In this figure it can be seen that the experimental arithmetic mean diameter D_{10} decreases while the radial location is increasing up to a certain minimum from which starts increasing again. The trend of the numerical results is similar, especially in the graphic of Fig. 9a, in which is possible to appreciate a minimum in D_{10}.

In Fig. 10, comparison between experimental and numerical Sauter mean diameter is shown.

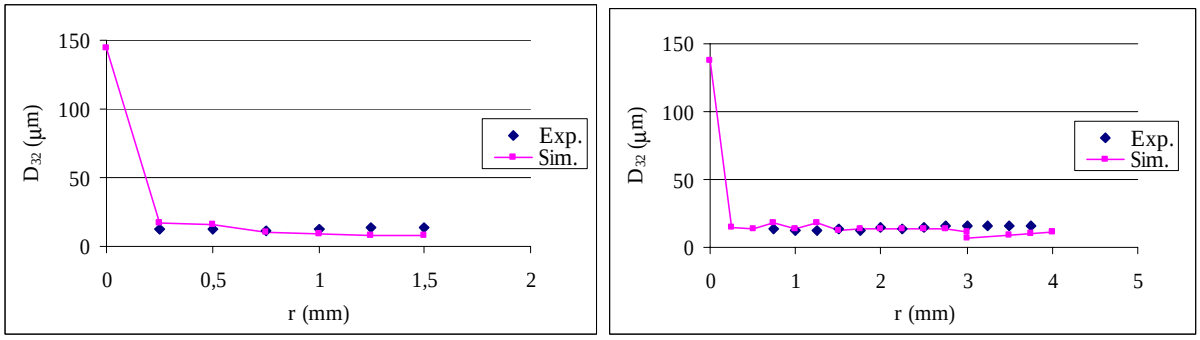

(a) $x/d_0 = 52$ and $t = 285$ µs (a) $x/d_0 = 120$ and $t = 445$ µs

Fig. 10. Comparison of Sauter mean diameter

It can be seen that the values are quite similar. The Sauter mean diameter is larger than the arithmetic one. In the numerical results, it can be seen a very high value at the axis of the spray and a fast decreasing following the experimental results. This is due to the high density of liquid in few blobs existing at the axis that makes the relation volume to surface very high.

As a conclusion, the numerical model has revealed as a strong and useful tool to study Diesel sprays to and to predict spray behavior in different working conditions.

5. References

[1] Reitz R D and Bracco F V 1984 Mechanisms of Breakup of Round Liquid Jets *Encyclopedia of Fluid Mechanics* **III**-11-Gas Liquid Flows GULF PUBLISHING

[2] Lefebvre A H 1989 Atomization and Sprays *Hemisphere Publishing Corp*

[3] Bayvel L and Orzechowsky Z 1993 Liquid Atomization *Taylor & Francis*

[4] Reitz R D 1987 Modeling Atomization Processes in High-Pressure Vaporising Sprays *Atomization Sprays Technol* **3**-309-37

[5] O'Rourke P J and Amsden A A 1987 The TAB Method for Numerical Calculation of Spray Droplet Breakup *SAE Paper 872089*
[6] Reitz R D and Diwakar R 1987 Structure of High-Pressure Fuel Sprays *SAE Paper No. 870598*
[7] Gonzalez M A, Lian Z W and Reitz R D 1992 Modeling Diesel Engine Spray Vaporization and Combustion *SAE Paper 920579*, 1064-76
[8] Patterson M A, Kong S C, Hampson G I and Reitz R D 1994 Modeling the Effects of Fuel Injection Characteriscs on Diesel Engine Soot and NOx Emissions *SAE Paper 940523*
[9] Xing J, Ricart L and Reitz R D 1998 Computer Modeling of Diesel Spray Atomization and Combustion *Combustion Sci. Technol*. **137**, 1-6, p.171
[10] Beale J C and Reitz R D 1999 Modeling spray atomization with the Kelvin-Helmholtz/Rayleigh-Taylor hybrid model *Atomization and Sprays* **9**
[11] Lee C H, and Reitz R D 1999 Modeling the effects of gas density on the drop trajectory and breakup size of high-speed liquid drops *Atomization and Sprays* **9**-497-517
[12] Putnam A 1961 Integrable Form of Droplet Drag Coefficient *ARS Journal* **131**-1467-8
[13] Sánchez M L 1996 Estudio de la estructura de un chorro atomizado intermitente mediante velocimetría de Desfase-Doppler *Tesis Doctoral*, Universidad de Valladolid
[14] Jiménez J E 2000 Estudio Experimental de un chorro atomizado intermitente y evaporativo *Tesis Doctoral*, Universidad de Valladolid